Supplementary information

Rejuvenating Propylene Carbonate-based Electrolytes by Regulating the Coordinated Structure toward All-Climate Long Lifespan Potassium-Ion Batteries

Zixing Wang[1], Kang Luo[1], Jian-Fang Wu[1], Peng Gao[1], Kexuan Wang[2], Shi Chen[2], Jian Tu[3], Xiulin Fan[4], Jilei Liu[1,*]

[1] School of Materials Science and Engineering, Hunan Joint International Laboratory of Advanced Materials and Technology of Clean Energy, Hunan Province Key Laboratory for Advanced Carbon Materials and Applied Technology, Hunan University, Changsha 410082, China

[2] Joint Key Laboratory of the Ministry of Education, Institute of Applied Physics and Materials Engineering, University of Macau, Avenida da Universidade, Taipa, Macau 999078, China

[3] LI-FUN Technology Corporation Limited, Zhuzhou 412000, Hunan, China

[4] State Key Laboratory of Silicon Materials, School of Materials Science and Engineering, Zhejiang University, Hangzhou 310027, Zhejiang, China

* **Corresponding author**. E-mails: liujilei@hnu.edu.cn.

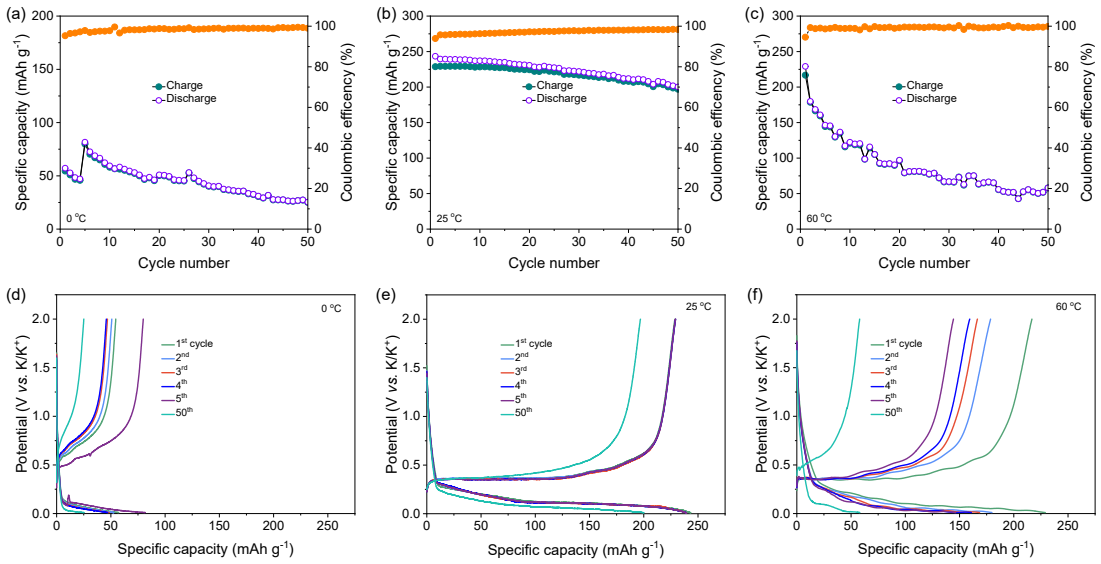

Figure S1. Cycling performance of graphite||K half-cells with commercial electrolytes at **(a)** 0 °C, **(b)** 25 °C and **(c)** 60 °C. Charge-discharge curves of graphite anode in the commercial electrolyte at **(d)** 0 °C, **(e)** 25 °C and **(f)** 60 °C.

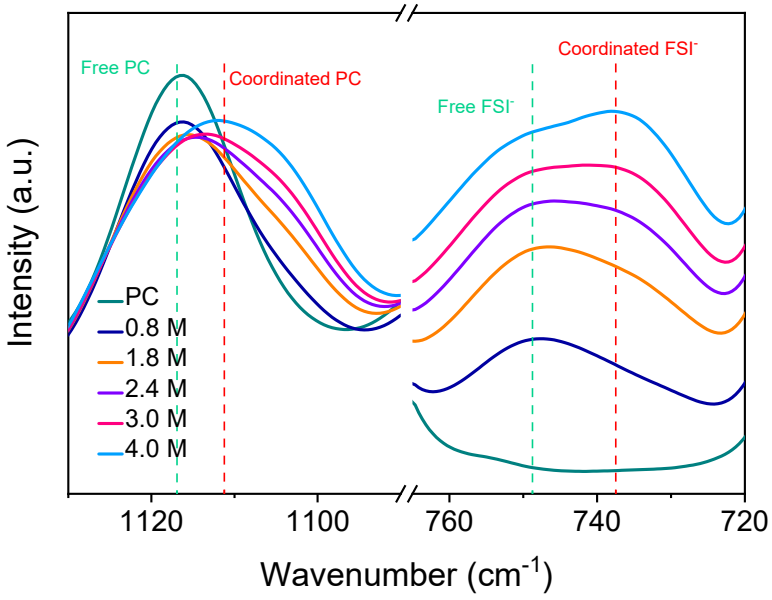

Figure S2. FTIR spectra of KFSI-PC electrolytes in the region from 720 to 1130 cm^{-1}.

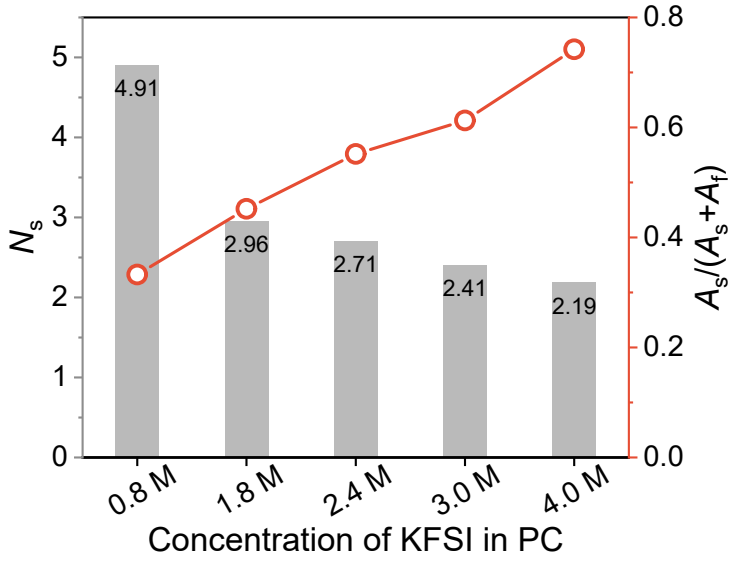

Figure S3. Relative area of coordinated PC solvent in KFSI mixtures and calculated coordination number in different concentrations of KFSI in PC electrolytes.

The relative areas of C=O band of PC (~712 cm^{-1}) and uncoordinated (~705 cm^{-1}) were used to estimate the concentration of PC molecules coordinated to the K^+ cation using this equation[1-3]:

$$C_s = NC_K$$

$$C_s = \frac{A_s}{A_s + A_f} C^0$$

$$N_s = \frac{A_s}{A_s + A_f} \frac{C^0}{C_K}$$

where C_s, C^o, and C_K are the concentrations of coordinated PC, total PC, and potassium salt, respectively, N_s is coordination number, and A_s and A_f are relative areas of the C=O bands for coordinated PC and uncoordinated PC, respectively.

As shown in **Figure S3**, the average solvation numbers are inversely related to the salt concentration. At low KFSI concentration, the solvation numbers for PC are ~4.9. At high KFSI concentration, the solvation numbers for PC are ~2.2.

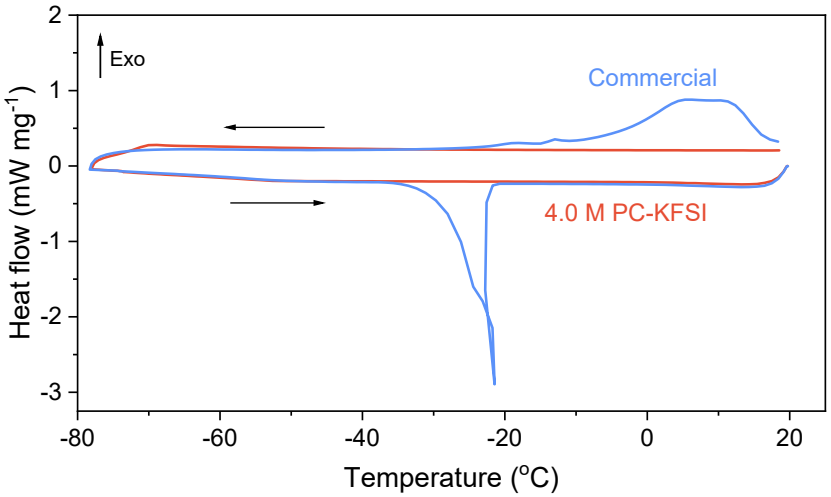

Figure S4. DSC curves of 4.0 M PC-KFSI and commercial electrolytes. Commercial electrolyte showed obvious exothermic peaks at 8 °C during cooling, which was assigned to the crystallization or solidification of the liquid samples. Instead, no exothermic or endothermic peak was observed for the 4.0 M PC-KFSI electrolyte, suggesting it can maintain fully liquid state within the measuring temperature range from −80 to 20 °C, which was attributed to the absence of free solvent in the concentrated electrolyte that makes it behave like ionic liquid.

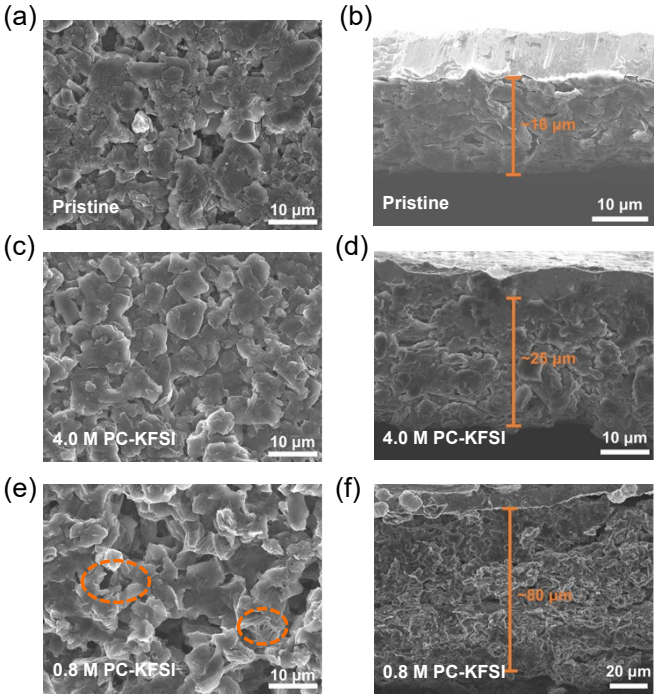

Figure S5. The SEM images of **(a, b)** pristine graphite, discharged in **(c, d)** 4.0 M PC-KFSI and **(e, f)** 0.8 M PC-KFSI.

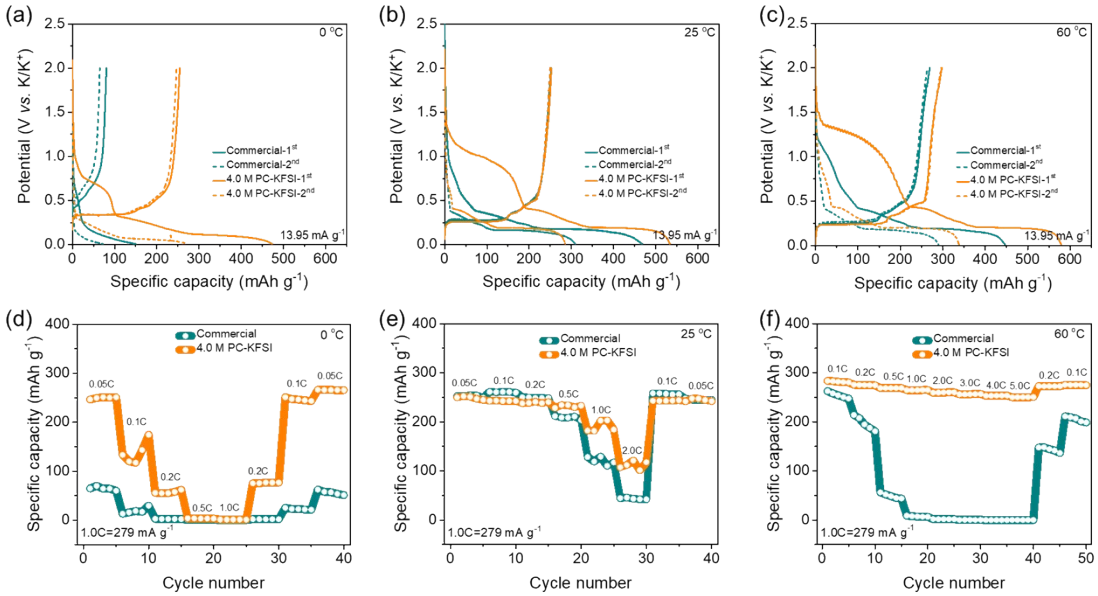

Figure S6. Charge-discharge curves of graphite||K half-cells with 4.0 M PC-KFSI electrolyte and commercial electrolytes at **(a)** 0 °C, **(b)** 25 °C and **(c)** 60 °C. The comparison of rate performance between 4.0 M PC-KFSI electrolyte and commercial electrolyte at **(d)** 0 °C, **(e)** 25 °C and **(f)** 60 °C.

At 25 °C, two electrolytes yielded a reversible capacity of approximately 250 mAh g^{-1} at 0.05 C rate. In contrast, at higher rates (1 C and 2 C), the commercial electrolyte showed a lower capacity than those of 4.0 M PC-KFSI. Cooling to 0 °C, the commercial electrolyte showed a low capacity and displayed rapid capacity fading with the current density increased, while the designed electrolyte still maintained a capacity of 250 mAh g^{-1} at 0.05 C. When tested at 60 °C, the capacities declined quickly in just a few cycles for commercial electrolytes. In contrast, 4.0 M PC-KFSI offered excellent rate performance for the graphite electrode (250 mAh g^{-1} at 5 C), demonstrating its suitability for battery operation in a much wider temperature range with significantly enhanced kinetics.

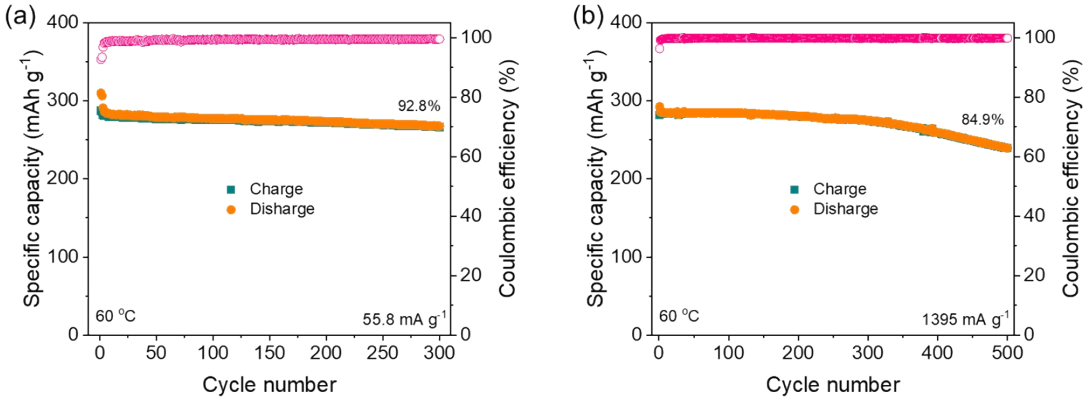

Figure S7. Cycling performance of graphite||K half-cells with 4.0 M PC-KFSI at 60 °C with the current density of **(a)** 55.8 mA g^{-1} and **(b)** 1395 mA g^{-1}.

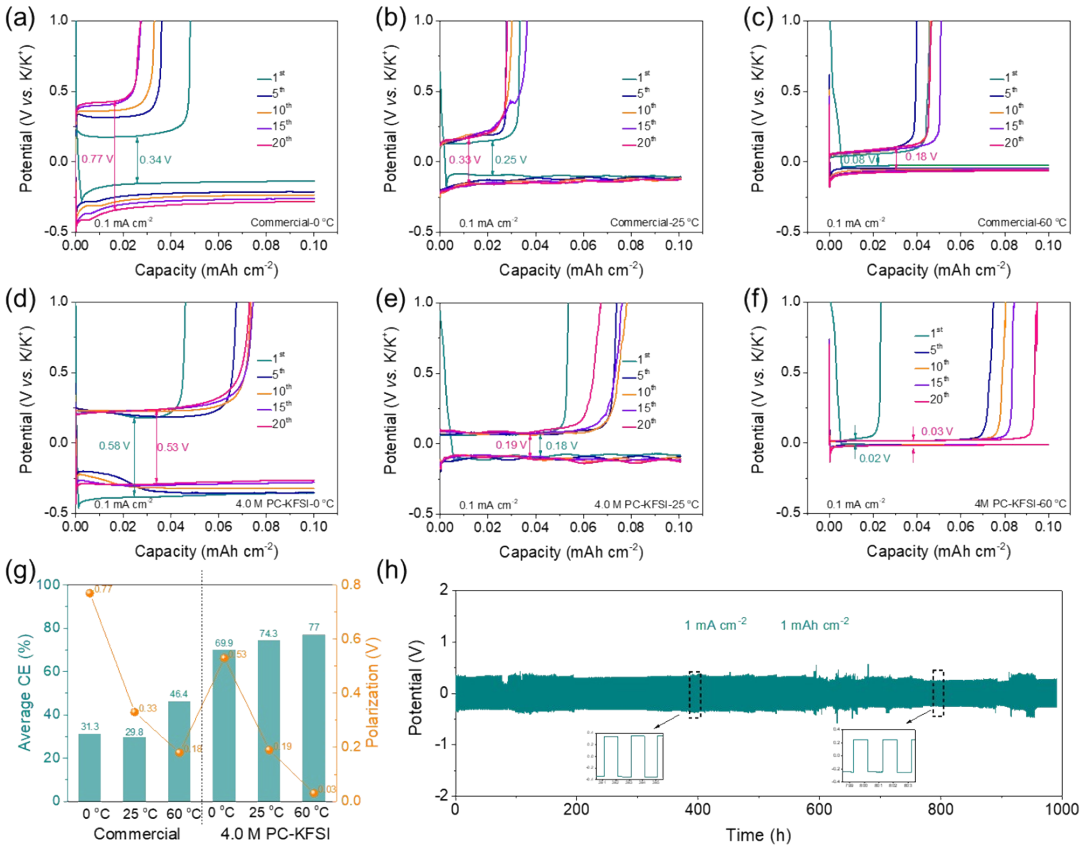

Figure S8. Voltage profiles of first 20 cycles in K||Cu cells with commercial electrolytes **(a)**-**(c)** and 4.0 M PC-KFSI **(d)**-**(f)** at different temperatures. **(g)** The comparison of average coulombic efficiency value and voltage polarization before the 20 cycles. **(h)** Cycling stability of K||K symmetric cells in 4.0 M PC-KFSI at 1.0 mA cm^{-2}.

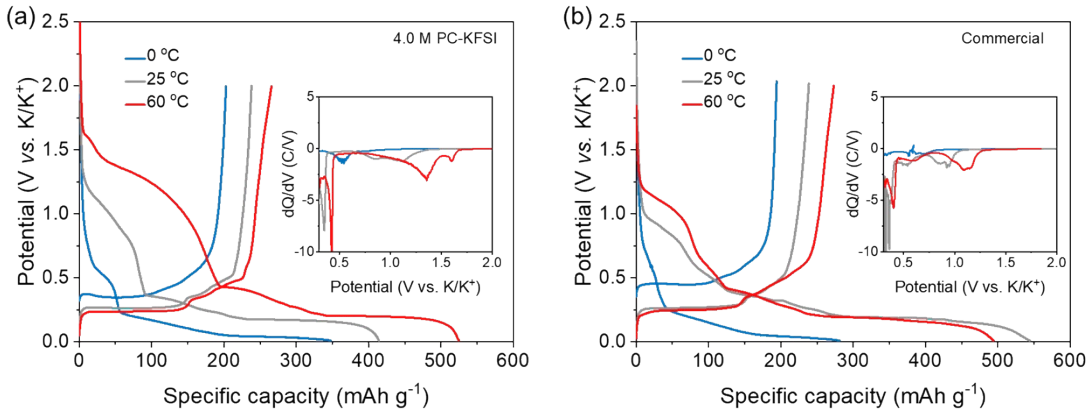

Figure S9. Initial charge-discharge curves of graphite||K half-cells with 4.0 M PC-KFSI electrolyte **(a)** and commercial electrolytes **(b)**. Inset showed the dQ/dVcurves.

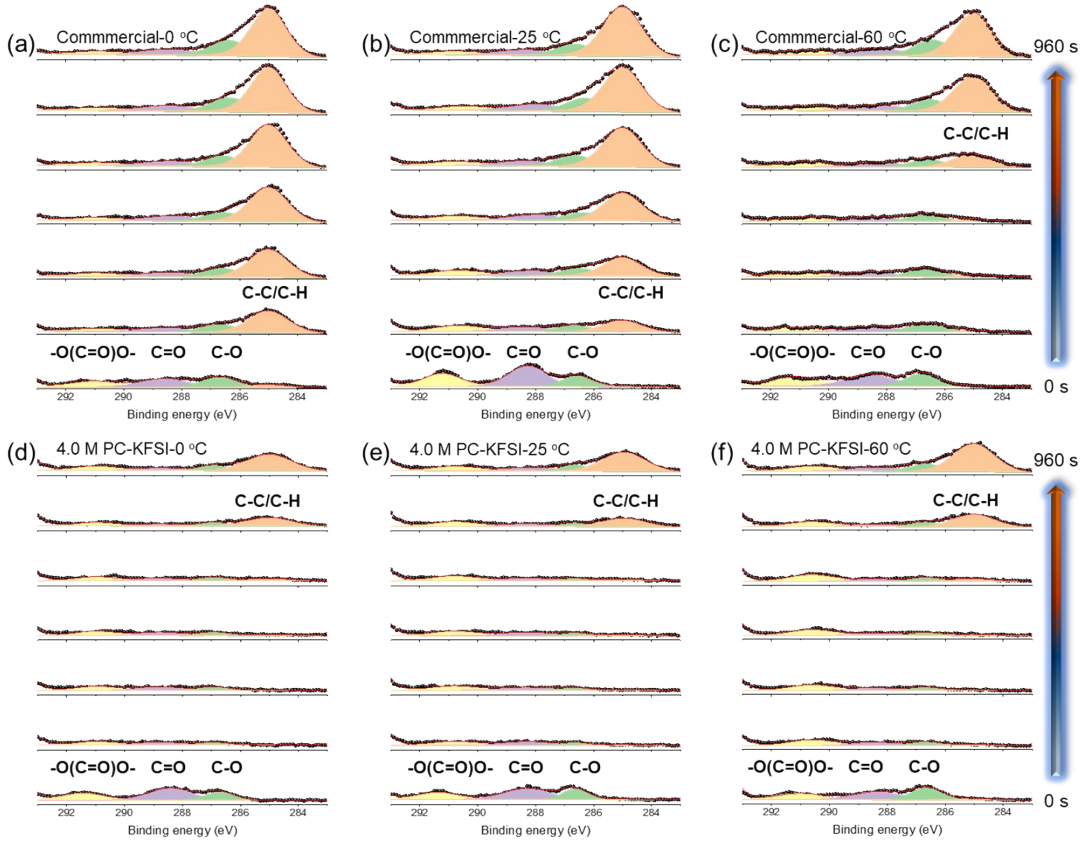

Figure S10. Depth profiling XPS analysis (Normalized according to the relative peak intensity of the XPS spectrum.) of C 1s spectra retrieved from Graphite||K half-cells with sputtering time from 0 to 960 s. **(a)** Commercial-0 °C, **(b)** Commercial-25 °C, **(c)** Commercial-60 °C, **(d)** 4.0 M PC-KFSI-0 °C, **(e)** 4.0 M PC-KFSI-25 °C and **(f)** 4.0 M PC-KFSI-60 °C.

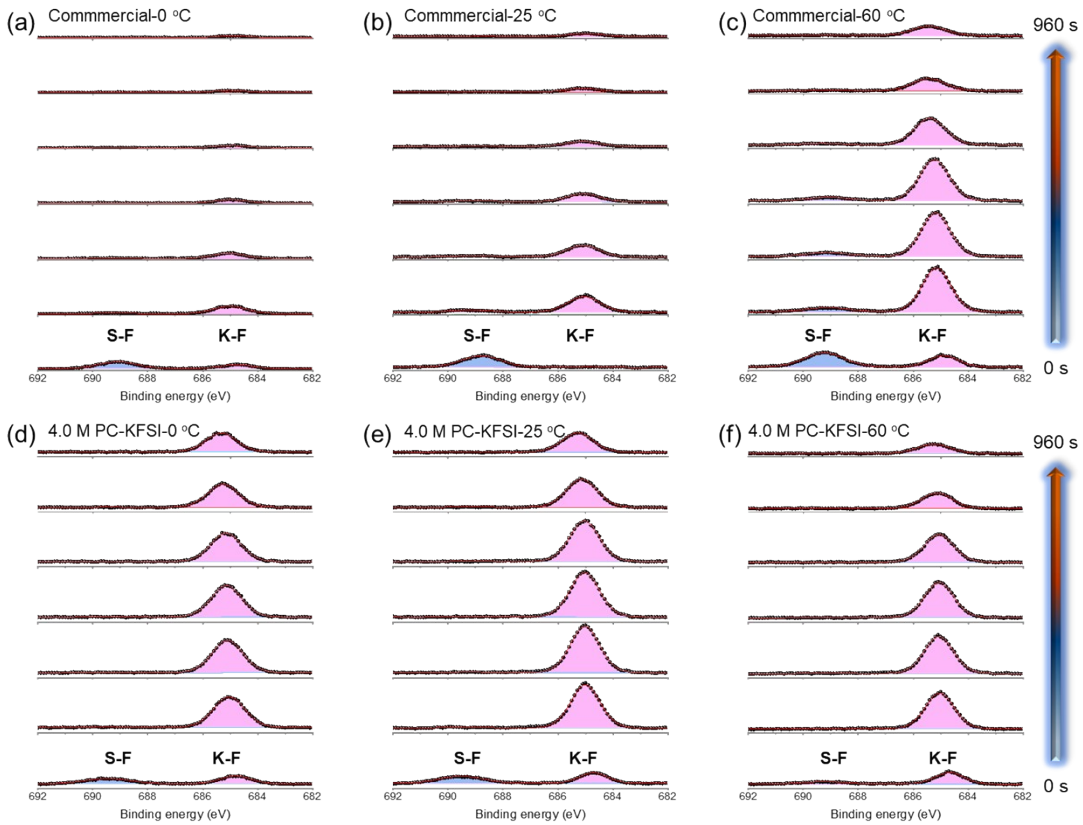

Figure S11. Depth profiling XPS analysis (Normalized according to the relative peak intensity of the XPS spectrum.) of F 1s spectra retrieved from Graphite||K half-cells with sputtering time from 0 to 960 s. **(a)** Commercial-0 °C, **(b)** Commercial-25 °C, **(c)** Commercial-60 °C, **(d)** 4.0 M PC-KFSI-0 °C, **(e)** 4.0 M PC-KFSI-25 °C and **(f)** 4.0 M PC-KFSI-60 °C.

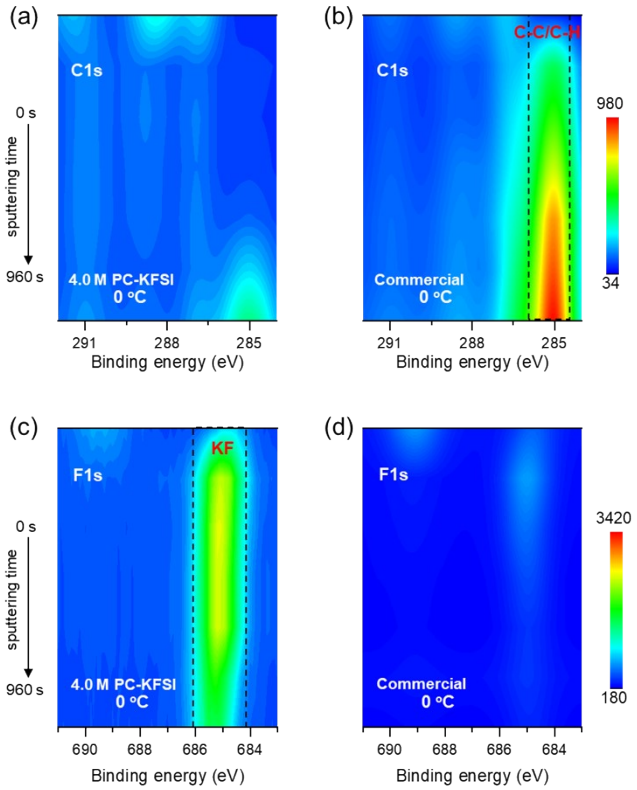

Figure S12. Contour plots of the XPS C1s and F1s of the pre-cycled graphite electrodes with **(a), (c)** 4.0 M PC-KFSI and **(b), (d)**commercial electrolytes at 0 °C.

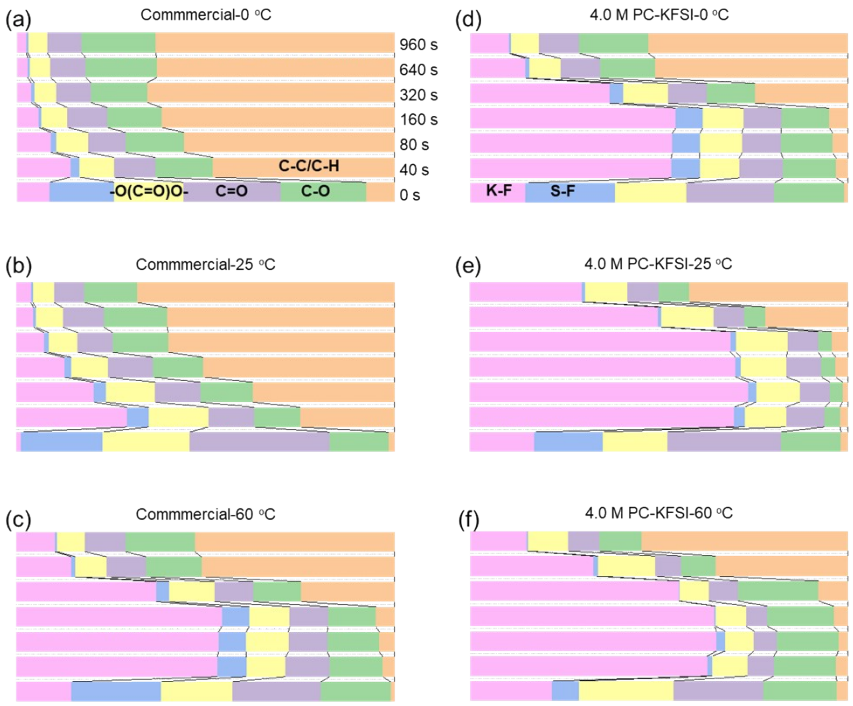

Figure S13. Normalized ratios of different species in the SEI formed in commercial electrolyte and 4.0 M PC-KFSI at different temperatures, respectively. **(a)** Commercial-0 °C, **(b)** Commercial-25 °C, **(c)** Commercial-60 °C, **(d)** 4.0 M PC-KFSI-0 °C, **(e)** 4.0 M PC-KFSI-25 °C and **(f)** 4.0 M PC-KFSI-60 °C.

To investigate how electrolyte changes the chemical compositions of the SEI at different temperatures, depth-profiling XPS experiments (a high-energy Ar^+ ion beam was used to sputter the cycled Gr electrode for 40, 80, 160, 320, 640, and 960 s) were performed on the Gr electrode in high-concentrated electrolytes and commercial electrolyte at 0 °C, 25 °C and 60 °C, respectively. The C 1s spectra can be deconvoluted into five peaks include C-C/C-H (~285 eV), C-O (~286.7 eV), C=O (~288.4 eV), -O(C=O)O- (~291.0 eV)[4-7]. The C-C/C-H bonds could be ascribed to SEI species like alkyl carbonate or ketjen black and graphite in the electrode; the C-O, C=O and -O(C=O)O- bonds are originated from organic and inorganic species of SEI such as poly (ethylene oxide) (PEO), potassium ethylene decarbonate (PEDC) and potassium carbonate (K_2CO_3)[6, 7]. Two peaks centered at 684.7 and 689.2 eV in F 1s spectra are assigned to K-F and X-F (O-F, S-F) bonds[4, 8]. The inner layer is mainly composed of KF that is due to KFSI decomposition, and the outer layer are formed by incomplete KFSI decomposition.

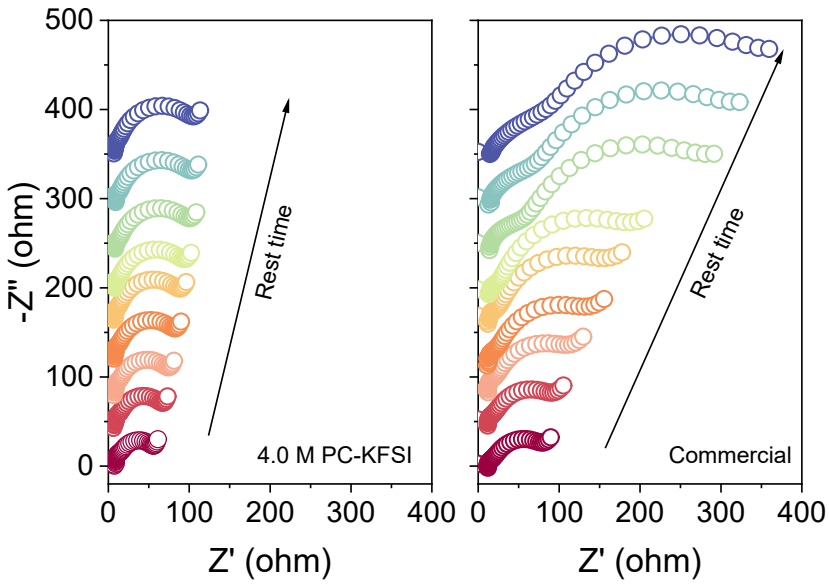

Figure S14. Nyquist plots of graphite||K half-cells with long-term resting at 60 °C.

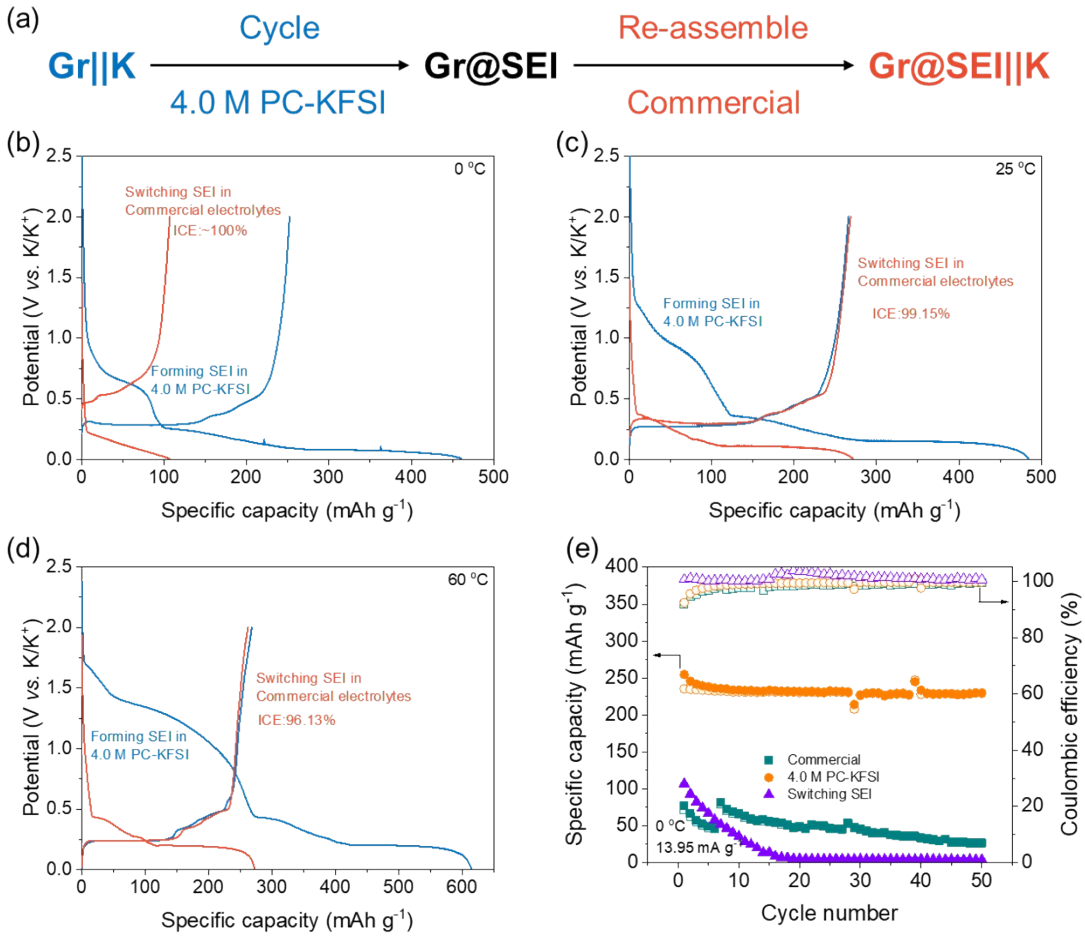

Figure S15. **(a)** Illustration of the exchange experiments. The comparation of initial charge-discharge curves of graphite||K half-cells with 4.0 M PC-KFSI electrolyte and switching electrolyte at **(b)** 0 °C, **(c)** 25 °C and **(d)** 60 °C. **(e)** The cycle performance of graphite anodes reassembled in different electrolytes at 0 °C.

Ming et al. proposed a concept of a switched electrolyte interface model, whereby an electrode was first cycled in a specific electrolyte to form a unique SEI, and this SEI-coated electrode was then used in another target electrolyte for better performance[9]. The Gr@SEI electrodes were prepared as follows. Firstly, the Gr||K half-cells were cycled once in the 4.0 M PC-KFSI electrolyte to form the Gr@SEI and then taken out after the cell was disassembled. The Gr@SEI was carefully cleaned and dried using PC solvents, and then assembled Gr@SEI||K half-cells using a commercial electrolyte (i.e., switching electrolyte).

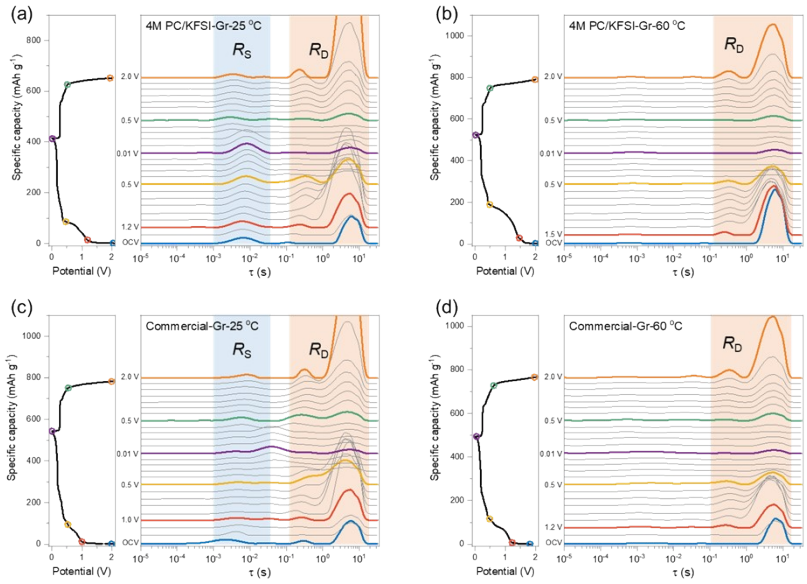

Figure S16. In-situ EIS during 1st charge-discharge process at 25 °C and 60 °C of graphite||K half-cells with **(a)**, **(b)** 4.0 M PC-KFSI and **(c)**, **(d)** Commercial electrolytes.

Three-electrode electrochemical impedance spectroscopy (EIS) with further the distribution of relaxation time (DRT) analysis was subsequently conducted for uncovering and separating the contribution of different processes to cell impedance. The impedance of K^+ crossing SEI (R_{SEI}, 10^{-3}-10^{-1} s), and the desolvation resistance (R_{ct}, 10^{-1}-10^{2} s) can be quantitatively separated.

The diffusion coefficient D_K was calculated according to Eq. 1[10]:

$$D_K = \frac{R^2T^2}{2A^2n^4F^4C^2\sigma^2} \quad (1)$$

R was the gas constant (8.314 J mol^{-1} K^{-1}), T was the experiment temperature (298 K), F was the Faraday constant (96487 C mol^{-1}), A (cm^2) was the surface area of the electrode sheet, n=1/8 mol, C=n/V_m. σ was the Warburg coefficient (the frequency f and the data of the real part Z' in the range of 1-0.01 Hz were selected, Z'-ω (ω=2πf) curve was drawn, and the slope of the fitted straight line was σ according to Eq. 2.

$$Z_{re} = R_\Omega + R_{ct} + \sigma w^{-1/2} \quad (2)$$

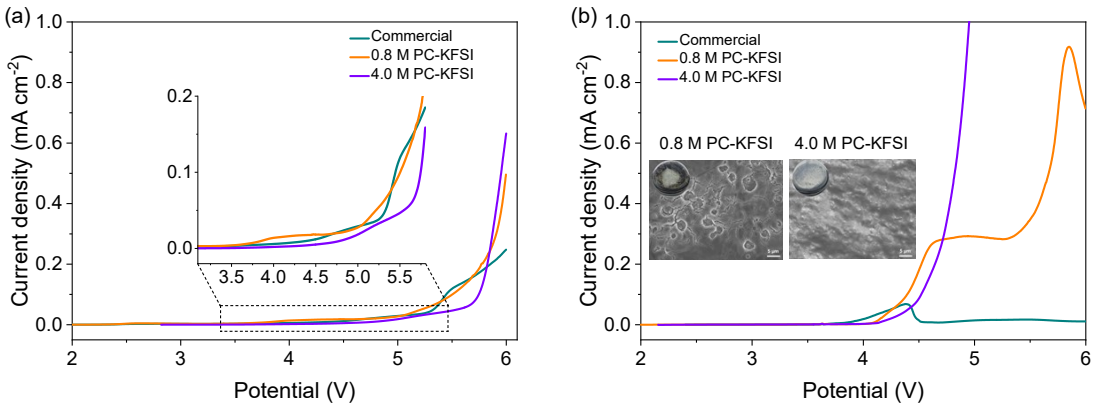

Figure S17. **(a)** Linear sweep voltammetry curves of different electrolytes. Inset in **(a)**: the magnification of the 3.2 V-5.8 V. **(b)** Oxidation stability of Al current collectors with different electrolytes. Inset in **(b)**: SEM images of the aluminum foils in different electrolytes.

It is known that the high voltage stability of conventional KFSI based electrolytes is restricted because they could corrode Al current collector severely. Thus, the linear sweep voltammetry (LSV) of K||Pt||K and K||Al cells were performed to investigate the oxidation stability and corrosion of Al foil with different electrolytes at high voltage (**Figure S16**). The electrochemical voltage windows of 4.0 M PC-KFSI, 0.8 M PC-KFSI and commercial electrolytes are 4.5, 3.6 and 4.3 V (**Figure S16a**), respectively, testifying that high-concentrated electrolyte will lead to a decrease of the antioxidant ability of the electrolytes. For the 0.8 M and 4.0 M PC-KFSI electrolytes, the onset corrosion voltages are 4.1 V and 4.3 V (**Figure S16b**), respectively, indicating the increased electrolyte concentration is conductive to suppressing the Al corrosion.

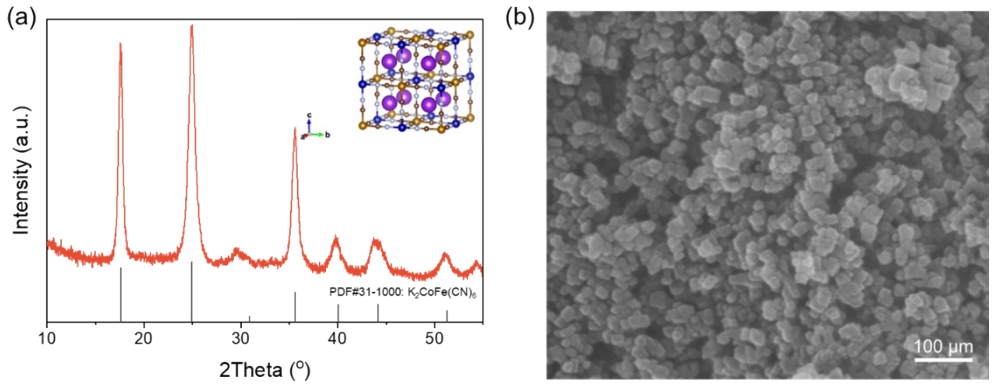

Figure S18. **(a)** XRD patterns and **(b)** SEM images of K-FeHCFe.

Prussian blue analogues (PBAs) are considered as superior cathode materials for PIBs because of their three-dimensional open framework structure, high stability, and low cost. Among the Prussian blue analogs, Prussian white theoretically contains one more extractable K-ion than Prussian blue in the open framework, which rendered double capacity during the initial charge in a full cell. Prussian white (K-FeHCFe) was synthesized via simple co-precipitation method at 0 °C. Firstly, 4 mmol $FeSO_4 \cdot 7H_2O$ was dissolved into 100 mL deionized water to form solution A. And 4 mmol $K_4Fe(CN)_6 \cdot 3H_2O$ was dissolved into 100 mL deionized water to form solution B. Then 16 mmol $K_3C_6H_5O_7 \cdot H_2O$ and 0.25 mol KCl were added into solution A. Solution B was added into solution A drop by drop with strong stirring, and immediately forming the milky white precipitates. Stirring for 2 h, then aging for 12 h. All the above processes were carried out under an appropriate argon atmosphere. The precipitates were collected by centrifugation, washed thoroughly with deionized water and then ethanol for three times, respectively. Then, the obtained precipitates were dried for 12 h under vacuum freezing. The specific surface area of the K-FeHCFe is 106.31 $m^2 g^{-1}$.

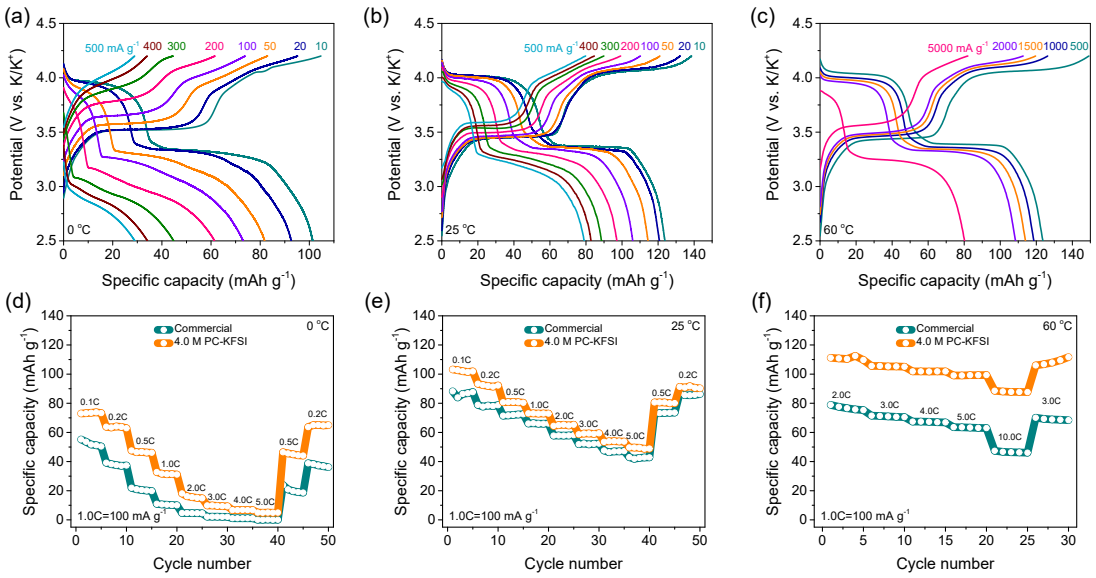

Figure S19. Charge-discharge curves of K-FeHCFe cathode in the 4.0 M PC-KFSI electrolyte with different current density at **(a)** 0 °C, **(b)** 25 °C and **(c)** 60 °C. The comparison of rate performance between high-concentrated electrolyte and commercial electrolyte at **(d)** 0 °C, **(e)** 25 °C and **(f)** 60 °C.

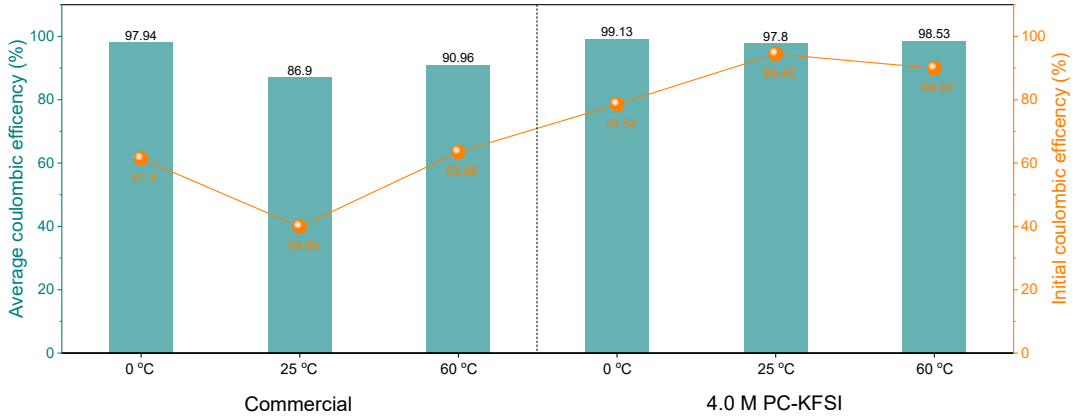

Figure S20. The comparison of average coulombic efficiency (first ten cycles) and initial coulombic efficiency between high-concentrated electrolyte and commercial electrolyte.

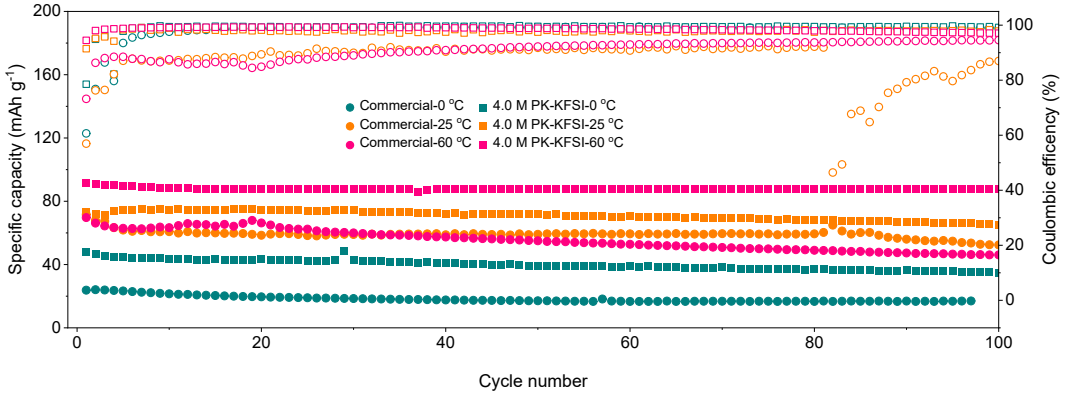

Figure S21. The comparison of cycling performance between high-concentrated electrolyte and commercial electrolyte at different temperatures.

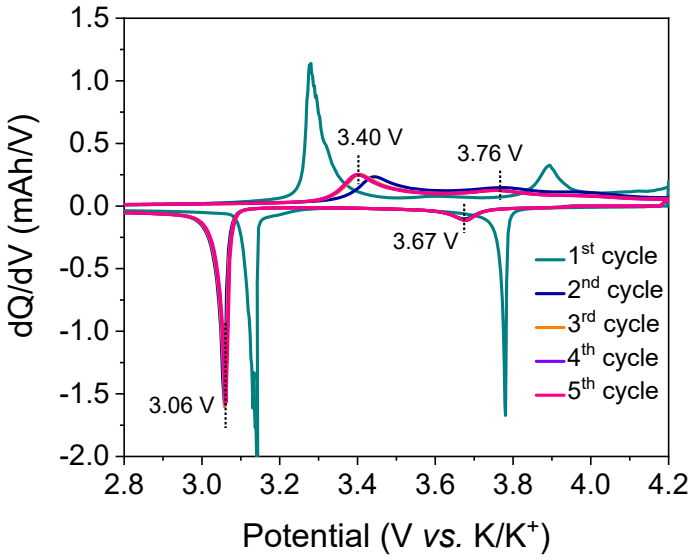

Figure S22. dQ/dV curves of the full cell.

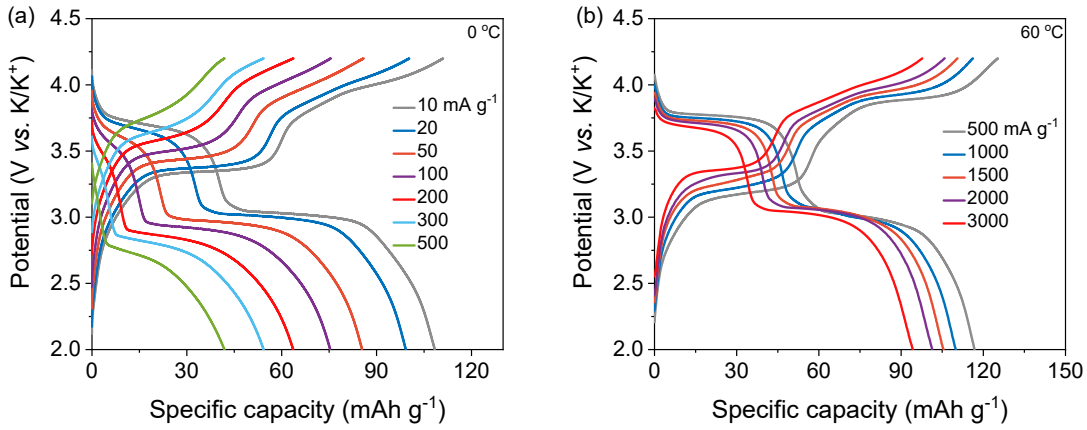

Figure S23. Rate performance of Gr||K-FeHCFe cells at **(a)** 0 °C and **(b)** 60 °C.

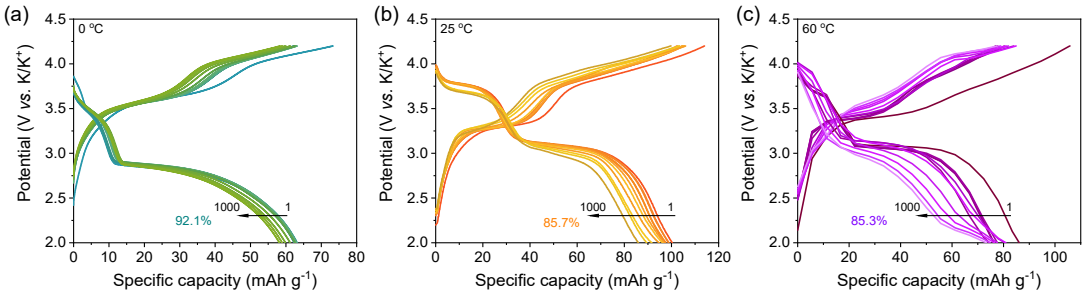

Figure S24. Charge-discharge profiles of graphite||K-FeHCFe full cells with high-concentrated electrolytes at 0-60 °C.

Table S1. The comparison of the graphite anode in concentrated electrolytes with other representative electrolytes.

Anode	Electrolytes	Reversible capacity ($mAh\ g^{-1}$ / $mA\ g^{-1}$)	Initial Coulombic efficiency (%)	Cycling stability (retention / cycles / $mA\ g^{-1}$)	Ref.
Graphite	0.8 M KPF_6/EC:DEC	273 / 6.975	57.4%	50.7% / 50 / 139.5	11
Graphite	1.0 M KPF_6/EC:PC	246 / 20	66.5%	89% / 200 / 20	12
Graphite	KFSI/EMC (1:2.5 MR)	-255 / 93	~60%	100% / 2000 / 93	13
Graphite	1.0 M KFSI/EC:DEC	~250 / 25 ~250 / 25 ~250 / 25	59%(PVDF) 79%(PANa) 89% (CMCNa)	/	14
Graphite	2.0 M KFSI/TEP	275 / 55.8 137 / 558	50.8%	79% / 1500 / 558	15
Graphite	1.0 M KPF_6/DME	108 / 280	87.4%	53.2% / 3800 / 2800	16
Graphite	2.76 mol kg^{-1} KFSI/DME-HFE	201.7 / 25	82.3%	99.2% / 300 / 25	17
Graphite	0.5 M KPF6/DEGDME	110 / 25	~90%	74.6% / 50 /25	5
Natural graphite	1.0 M KFSI/DEGDME	105 / 500 77.8 / 10000	~63%	88.5% / 100 / 2000	18
Expanded Graphite	1.0 M KFSI/EC:DEC	~263 / 10	81.56%	~100% / 500 / 200	19
Expanded Graphite	0.5 M KPF6/EC:DEC	226.8 / 100	52.57%	72.3% / 200 / 100	20
Graphite (0 °C)	**4.0 M KFSI/PC**	**254.26 / 13.95**	**53.73%**	**96.6% / 150 / 13.95**	**This work**
Graphite (25 °C)		**254.36 / 13.95**	**61.63%**	**93.6% / 400 / 55.8**	
Graphite (60 °C)		**298.05 / 13.95**	**51.45%**	**99.0% / 500 / 1116**	

Table S2. The comparison of the KFeHCF//Gr full cell with other KIB full cell systems.

Full cells	Working voltage (V)	Reversible capacity (mAh g^{-1} / mA g^{-1})	Energy density (Wh kg^{-1})	Cycling stability (retention / cycles / mA g^{-1})	Ref.
KNiHCF//Gr	2.84	62.1 / 100	96.54	87.1% / 500 /500	21
KMnHCF//Gr	3.58	145 / 15	331.5	98.5% / 300 / 30	22
KMnHCF//Gr	3.50	110 / 30	240.8	73% / 60 / 30	23
KMnHCF//Gr	2.90	80 / 50	~116	~100% / 60 / 50	24
KFeHCF//Super P	2.20	65 / 100	76.6	93.4% / 50 / 100	25
PTCDA@450 °C//SC	~1.60	116 / 50	101.2	65% / 3000 / 600	26
KVPF//VPO_4	3.10	101 / 50	208.7	86% / 300 / 50	27
KVPF@C//SC	3.66	95.1 / 50	235.5	80.3% / 500 / 50	28
$KMnO_2$//HSC	1.80	121 / 100	138.6	80% / 500 / 1000	29
KCO@KMO//SC	~2.00	101 / 10	220	88.7% /100 / 10	30
$KCoO_2$//HC	~2.00	72 / 30	102.6	78.2% / 100 / 30	31
$KFeC_2O_4F$//SC	2.85	85 / 100	161.5	~100% / 200 / 100	32
KVP//PANI-LT	3.06	77.8 / 20	148.6	~81.9% / 600 / 100	33
Graphite (0 °C)	**3.35**	**109.5 / 10**	**203.8**	**92.1% / 1000 / 200**	**This work**
Graphite (25 °C)	**3.45**	**128.1 / 20**	**245.5**	**78.2% / 2000 / 200**	
Graphite (60 °C)	**3.40**	**116.9 / 500**	**220.8**	**85.3% / 1000 / 2000**	

The energy density was calculated based on the total mass of cathode and anode materials.

References

1. D. M. Seo, S. Reininger, M. Kutcher, K. Redmond, W. B. Euler and B. L. Lucht, *J.Phys. Chem. C*, 2015, **119**, 14038-14046.

2. X. Liu, X. Shen, H. Li, P. Li, L. Luo, H. Fan, X. Feng, W. Chen, X. Ai, H. Yang and Y. Cao, *Adv. Energy Mater.*, 2021, **11**, 2003905.

3. X. Liu, X. Shen, L. Luo, F. Zhong, X. Ai, H. Yang and Y. Cao, *ACS Energy Lett.*, 2021, **6**, 4282-4290.

4. J. Zhang, J.-F. Wu, Z. Wang, Y. Mo, W. Zhou, Y. Peng, B. He, K. Xiao, S. Chen, C. Xu and J. Liu, *J. Energy Chem.*, 2022, **71**, 344-350.

5. Y. Lei, D. Han, J. Dong, L. Qin, X. Li, D. Zhai, B. Li, Y. Wu and F. Kang, *Energy Storage Mater.*, 2020, **24**, 319-328.

6. W. Zhou, B. He, L. Quan, R. Li, Y. Chen, C. Fan, S. Chen, C. Xu, X. Fan, L. Xing and J. Liu, *Adv. Energy Mater.*, 2022, **13**, 2202874.

7. Y. Mo, W. Zhou, K. Wang, K. Xiao, Y. Chen, Z. Wang, P. Tang, P. Xiao, Y. Gong, S. Chen, P. Gao and J. Liu, *ACS Energy Lett.*, 2023, **8**, 995-1002.

8. M. Gu, L. Fan, J. Zhou, A. M. Rao and B. Lu, *ACS Nano*, 2021, **15**, 9167-9175.

9. G. Liu, Z. Cao, P. Wang, Z. Ma, Y. Zou, Q. Sun, H. Cheng, L. Cavallo, S. Li, Q. Li and J. Ming, *Adv. Sci.*, 2022, **9**, e2201893.

10. C. Ho, I. Raistrick and R. J. J. o. T. E. S. Huggins, *J. Electrochem. Soc.*, 1980, **127**, 343.

11. Z. Jian, W. Luo and X. Ji, *J. Am. Chem. Soc.*, 2015, **137**, 11566-11569.

12. J. Zhao, X. Zou, Y. Zhu, Y. Xu and C. Wang, *Adv. Funct. Mater.*, 2016, **26**, 8103-8110.

13. L. Fan, R. Ma, Q. Zhang, X. Jia and B. Lu, *Angew. Chem. Int. Ed.*, 2019, **58**, 10500-10505.

14. S. Komaba, T. Hasegawa, M. Dahbi and K. Kubota, *Electrochem. Commun.*, 2015, **60**, 172-175.

15. S. Liu, J. Mao, Q. Zhang, Z. Wang, W. K. Pang, L. Zhang, A. Du, V. Sencadas, W. Zhang and Z. Guo, *Angew. Chem. Int. Ed.*, 2020, **59**, 3638-3644.

16. L. Wang, J. Yang, J. Li, T. Chen, S. Chen, Z. Wu, J. Qiu, B. Wang, P. Gao, X. Niu and H. Li, *J.Power Sources*, 2019, **409**, 24-30.

17. L. Qin, N. Xiao, J. Zheng, Y. Lei, D. Zhai and Y. Wu, Adv. Energy Mater., 2019, **9**, 1902618.

18. L. Li, L. Liu, Z. Hu, Y. Lu, Q. Liu, S. Jin, Q. Zhang, S. Zhao and S. L. Chou, *Angew. Chem. Int. Ed.*, 2020, **59**, 12917-12924.

19. Y. An, H. Fei, G. Zeng, L. Ci, B. Xi, S. Xiong and J. Feng, *J. Power Sources*, 2018, **378**, 66-72.

20. X. Li, Y. Lei, L. Qin, D. Han, H. Wang, D. Zhai, B. Li and F. Kang, *Carbon*, 2021, **172**, 200-206.

21. L. Li, Z. Hu, Y. Lu, C. Wang, Q. Zhang, S. Zhao, J. Peng, K. Zhang, S. L. Chou and J. Chen, *Angew. Chem. Int. Ed.*, 2021, **60**, 13050-13056.

22. L. Deng, J. Qu, X. Niu, J. Liu, J. Zhang, Y. Hong, M. Feng, J. Wang, M. Hu, L. Zeng, Q. Zhang, L. Guo and Y. Zhu, *Nat. Commun.*, 2021, **12**, 2167.

23. X. Bie, K. Kubota, T. Hosaka, K. Chihara and S. Komaba, *J. Mater. Chem. A*, 2017, **5**, 4325-4330.

24. Y.-H. Zhu, X. Yang, D. Bao, X.-F. Bie, T. Sun, S. Wang, Y.-S. Jiang, X.-B. Zhang, J.-M. Yan and Q. Jiang, *Joule*, 2018, **2**, 736-746.

25. C. Zhang, Y. Xu, M. Zhou, L. Liang, H. Dong, M. Wu, Y. Yang and Y. Lei, *Adv. Funct. Mater.*, 2017, **27**, 1604307.

26. L. Fan, R. Ma, J. Wang, H. Yang and B. Lu, *Adv. Mater.*, 2018, **30**, e1805486.

27. J. Liao, Q. Hu, X. He, J. Mu, J. Wang and C. Chen, *J. Power Sources*, 2020, **451**, 227739.

28. J. Liao, X. Zhang, Q. Zhang, Q. Hu, Y. Li, Y. Du, J. Xu, L. Gu and X. Zhou, *Nano Lett.*, 2022, **22**, 4933-

4940.
29. B. Lin, X. Zhu, L. Fang, X. Liu, S. Li, T. Zhai, L. Xue, Q. Guo, J. Xu and H. Xia, *Adv. Mater.*, 2019, **31**, e1900060.
30. S. Zhao, Z. Liu, G. Xie, Z. Guo, S. Wang, J. Zhou, X. Xie, B. Sun, S. Guo and G. Wang, *Energy Environ. Sci.*, 2022, **15**, 3015-3023.
31. T. Deng, X. Fan, C. Luo, J. Chen, L. Chen, S. Hou, N. Eidson, X. Zhou and C. Wang, *Nano Lett.*, 2018, **18**, 1522-1529.
32. B. Ji, W. Yao, Y. Zheng, P. Kidkhunthod, X. Zhou, S. Tunmee, S. Sattayaporn, H. M. Cheng, H. He and Y. Tang, *Nat. Commun.*, 2020, **11**, 1225.
33. J. Liao, C. Chen, Q. Hu, Y. Du, Y. He, Y. Xu, Z. Zhang and X. Zhou, *Angew. Chem. Int. Ed.*, 2021, **60**, 25575-25582.